Simulation of the Dynamics of Depth Filtration of Non-Brownian Particles

V. N. Burganos
Institute of Chemical Engineering and High Temperature Chemical Processes—Foundation for Research and Technology Hellas, GR-26500, Patras, Greece

E. D. Skouras, C. A. Paraskeva, and A. C. Payatakes
Institute of Chemical Engineering and High Temperature Chemical Processes—Foundation for Research and Technology Hellas, GR-26500, Patras, Greece
and
Dept. of Chemical Engineering, University of Patras, GR-26500, Patras, Greece

A new simulator for flow of aqueous suspensions and deposition of non-Brownian particles in granular media can predict the pattern of deposition and concomitant reduction in permeability as functions of depth, time and system parameters. The porous structure of the granular medium represented as a 3-D network of constricted pores considers the converging–diverging character of flow within pores. Using Lagrangian-type simulation the particle deposition rate was calculated. Gravity and drag, as well as hydrodynamic and physicochemical interactions between suspended particles and pore walls, were considered in calculating 3-D particle trajectories. Deposit configurations were computed, and the evolution of the pore structure was simulated at discrete time steps. Changes in the pore geometry and nature of the collector surface affect flow and trajectory computations directly. Clusters of deposited particles were allowed to become reentrained if exposed to shear stress higher than a critical value. Reentrained clusters, which moved through downstream pores, might redeposit downstream at suitable sites and cause clogging of sufficiently narrow pores. Particle clusters clogging pores have a finite permeability, which significantly affects the system's transient behavior. Clogged pores act as collectors of solitary particles and of reentrained clusters, and substantially affect the transient behavior of the filter. The loss of permeability was monitored by calculating pore and network hydraulic conductance at each time step. Numerical results for the loss of permeability, temporal evolution of filter efficiency, and specific deposit profiles are based on suspension flow simulations in a typical granular porous medium.

Introduction

Flow of suspensions through granular media is of particular importance in several processes of practical interest, such as depth filtration in granular beds, with applications in the tertiary treatment of wastewater, as well as the removal of Brownian ($d_p < 0.5\ \mu$m) and non-Brownian particles ($0.5\ \mu\text{m} < d_p < 30\ \mu$m) from process water and other industrial fluids (such as feedstock to catalytic crackers). It is also encountered in oil and gas recovery by flooding processes, where reduction of permeability, caused by the reentrainment, migration, and redeposition of fine particles (clay, and so on), is frequently a serious problem (McDowell-Boyer et al., 1986; Nabzar et al., 1996; Chauveteau et al., 1998). It is important to note that the majority of experimental and theoretical works concerning the process under consideration have appeared in connection with depth filtration (for recent reviews, see Ryan and Elimelech, 1996; Sahimi et al., 1990; Tien, 1989).

When an aqueous suspension of particles flows through a porous medium, such as a granular filter, particles deposit on the grain surfaces, gradually forming sizable deposits. The gradual growth of such deposits causes considerable reduction of the permeability, along with a drastic change (usually

Correspondence concerning this article should be addressed to A. C. Payatakes.

a monotonic decrease, but—in certain cases—an initial increase followed by a drastic decrease) of the deposition efficiency. Thus, the process is strongly transient.

To quantify the effects of the particle deposits on the permeability and the rate of particle deposition, one must know the forms and locations of the deposits. Notable experimental efforts to study the morphology of particle deposits were reported by Stein (1940), Cleasby and Baumann (1962), Maroudas and Eisenklam (1965), Ison and Ives (1969), and Payatakes et al. (1981). In general, the morphology of the deposits depends on several factors, including particle size, particle shape and density, particle structure (compact particle, agglomerate, floc, and so on), particle-to-wall, and particle-to-particle adherence. The latter renders the morphology a function of the Hamaker constant, the zeta potential, the concentration and valence of ions and counterions in the liquid, pH, the type and concentration of polyelectrolytes, the geometry and topology of the pore network, and the prevailing flow conditions. Another important key factor in determining the morphology of deposits is their behavior under flow-induced stress. Payatakes et al. (1977) and Tien and Payatakes (1979) pointed out the distinctly different behavior of deposits that are deformable, such as flocs, and deposits that are ''crumbly,'' such as those composed of solid particles held together by the Hamaker force. Deformable deposits are capable of being deformed continuously and irreversibly without rupture. Thus, they undergo gradual deformations, caused by the shear stress of the flow, and form sheaths of nearly uniform thickness on the collector walls, which, in turn, cause a moderate decrease in the permeability. This is the case of deposits formed by flocs that are made up of smaller compact particles held together by metalhydroxocomplexes (Stein, 1940; Maroudas and Eisenklam, 1965). On the other hand, compact particles (for example, clay) form deposits of variable thickness, depending on the local rate of deposition. These deposits are highly porous, and their packing density decreases as the adherence of the particles increases. Such deposits are crumbly rather than plastic and undergo frequent catastrophic changes, specifically, reentrainment of relatively large particle clusters that redeposit at suitable downstream sites (usually, constrictions). This process creates elaborate deposit formations, such as ''pendants'' and ''pouches,'' and causes frequent pore clogging along with a strong decrease in the permeability (Payatakes et al., 1981). A comprehensive discussion of deposit morphology is given in Payatakes et al. (1977, 1981), Pendse et al. (1978), Tien et al. (1979), and Tien (1989).

Several theoretical models of the transient behavior of particle deposition from aqueous suspensions in granular porous media have been proposed in the literature. These works have contributed significantly to the development of a quantitative *mechanistic* model of the transient behavior of the process under consideration. A few comments on the proposed algorithms and models are given below.

The first attempts to model the transient behavior of deep-bed filtration systems were made by Payatakes et al. (1977) and Tien et al. (1979). The granular medium in these works was represented as an ensemble of unit-bed elements (UBE), an approach originally proposed by Payatakes et al. (1973) and successfully employed to describe the initial stages of the filtration process (for a review, see Tien, 1989). Each UBE might include a number of constricted-tube-type cells (Payatakes et al., 1974a; Chiang and Tien, 1985), or a number of collectors surrounded by liquid envelopes, known as grain-in-cell models (Rajagopalan and Tien, 1976). Three key features were taken into account in these works, namely, the physicochemical interactions between particles and grain surfaces (or, equivalently, pore walls), the pattern of particle deposition on the collector surfaces, and the nature of the response of particle deposits to the flow-induced stresses. The theoretical results of Payatakes et al. (1977), based on the assumption of smooth coating, compared well with data obtained from experiments with flocs. Also, the constriction clogging assumption was confirmed by filtration experiments with suspensions of nonporous particles. Tien et al. (1979) presented an analysis that contained simulations for a complete filter. Direct comparison of these simulation results with the experimental data of Ives (1961), Camp (1964), Rimer (1968) and Deb (1969) showed that this type of simulator could be used to provide an order-of-magnitude estimate on a truly predictive basis.

Chiang and Tien (1985) used constricted tubes as collectors and employed the concept of UBE in their analysis. They considered two limiting situations. Particle deposits were formed in a rather uniform fashion and were allowed to grow in thickness with time. In addition, the authors used a stochastic simulation method and the concept of adhesion probability to calculate the rate of particle deposition in each unit cell. Unfortunately, this model cannot describe a complete filter cycle, as it does not deal with the problem of pore clogging and the concomitant decrease in permeability.

Mackie et al. (1987) developed a mathematical model to describe the evolution of the deposit on spherical grains. Calculated effluent concentration profiles and overall filter coefficients were found to be in qualitative agreement with experimental data for the initial stages of deposition. Unfortunately, the sphere-in-cell model used by these authors cannot be used for advanced stages of filtration, when particle-cluster reentrainment can significantly affect the overall filter coefficient and the permeability of the medium. However, their model was a highly useful effort for developing a mathematical tool for the description of the evolution of particle deposits on grain surfaces. The prediction of the evolution of the deposits was found to agree qualitatively with the experimental observations of Ushiki and Tien (1984) and Yoshida and Tien (1985), who reported the formation of ''caps'' on the upstream side of the grains, albeit using aerosols (rather than hydrosols).

Choo and Tien (1995a) developed a mathematical model similar to that of Mackie et al. (1987), again based on the concept of the sphere-in-cell model. Their model predicts that the deposited layer has nonuniform thickness and covers the entire surface of the grains. An important feature of this model was the consideration of porous deposits that allowed flow through them. A fairly good agreement with experimental data was observed. The same authors also presented another approach (Choo and Tien, 1995b), based on the UBE concept, and assumed that each element contained a number of cylindrical tubes of various sizes. It is known, however, that the assumption of straight capillary tubes oversimplifies the pore structure, leading to substantial underestimation of the rate of particle deposition in each cell (Payatakes et al.,

1974b). Moreover, such a pore geometry lacks the highly important feature of converging–diverging flow in the space between the grains. [This feature is particularly important because it accounts for pore clogging in a realistic way, according to the experimental observations in Payatakes et al. (1981).]

Putnam and Burns (1997) used stochastic simulation methods to calculate the effect of noncoagulating deposited particles on the collection efficiency of sphere-in-cell systems. Only single-layer deposition was allowed, and deposited particles were assumed to hinder particle capture on downstream surfaces. Comparison of their simulation results with data obtained from filtration experiments revealed fair qualitative but not quantitative agreement.

Recently, Bai and Tien (2000) used a set of macroscopic phenomenological equations to describe the filtration process and to describe the temporal evolution of the filter coefficient. Although the parameters involved in the set of macroscopic equations relate to physical quantities, their evaluation is not trivial, as they depend on a host of variables that affect the process. This approach is of significant value in the systematic description of experimental data for scale-up and process control purposes, but it is not a mechanistic model (or simulator) and so lacks genuine predictive capability.

Unfavorable surface interactions between particles and grain surfaces were considered by Bai and Tien (1996, 1999, 2000) and Vaidyanathan and Tien (1991), and were found to play a significant role in the estimation of the particle deposition rate. The extent of particle deposition under conditions of unfavorable surface interactions was investigated by Bai and Tien (1999), and a comparison was made with the experimental results of Vaidyanathan and Tien (1989), Elimelech and O'Melia (1990), and Elimelech (1992). The correlation equation presented in that work was found to follow closely their experimental findings as well as earlier experimental work.

Elimelech and coworkers (Ryan and Elimelech, 1996; Liu et al., 1995; Song and Elimelech, 1993; Elimelech, 1992 and 1994; Johnson and Elimelech, 1990; Elimelech and O'Melia, 1990) focused their attention on the nature and the size of surface forces, and formulated algorithms and models to calculate the particle deposition rate in sphere-in-cell systems. These publications are quite detailed in the consideration of colloid particle mobilization and deposition on the collector surface, but they do not give a predictive model for the loss of permeability at advanced stages of deposition. Rather, they examine different types of surface interaction and try to elucidate the role of particle deposits on the evolution of the filter coefficient at early stages of filtration.

Pore networks have found extensive use as models of the void space of granular media, and offered the flexibility required to bypass the UBE approximation. A review of network models for the study of particle motion and deposition in porous media was provided by Sahimi et al. (1990). A significant advantage of pore networks is the fact that they offer a satisfactory representation of the void space of the porous medium, which can be further improved by employing the constricted-tube geometry for the individual pores. In this way, the converging–diverging character of flow between the grains can be recovered very efficiently. An additional advantage of the network approach compared to the UBE approximation is that it can predict particle motion and deposition in directions other than that of the macroscopic flow. Visual observations by Payatakes et al. (1981) and Yoshida and Tien (1985) revealed that a large portion of particle deposits is caused by lateral flow streams, that is, by flow in pores that are not aligned with the mean flow direction. Particle transport and particle deposition in networks of pores have been described by Imdakm and Sahimi (1987, 1991), Sahimi and Imdakm (1991), Sharma and Yortsos (1987a,b), and Rege and Fogler (1987, 1988). All these works have contributed significantly to the understanding of the particle transport and deposition phenomena, using the pore network approach. However, the use of cylindrical tubes for the representation of the unit collectors may lead to large underestimation of the actual particle deposition rate, as shown by Payatakes et al. (1974b) (for vertical cylindrical pores) and Paraskeva et al. (1991) and Burganos et al. (1992a)) (for inclined cylindrical pores). Furthermore, the problem of pore clogging and permeability reduction, caused by the gradual growth of particle deposits, was not addressed, and only some limiting cases were considered, including the straining mechanism and the concomitant sieving activity. Straining appears when the size of the suspended particles is sufficiently large to cause clogging of narrow pores or even to prohibit entrance into a subset of the pore domain. A stochastic model of depth filtration by straining in granular beds was proposed by Payatakes (1973); see also Tien and Payatakes (1979) and Tien (1989). This model shows that straining becomes the dominant capture mechanism when the particle diameter d_p becomes comparable to ca. 15% of the mean grain diameter. Experiments performed by Chidaglia et al. (1996a,b) in columns randomly filled with identical glass spheres showed that the main capture mechanism was sieving, as a result of the geometrical structure of the filter. The size of suspended particles was in the range of 600–800 μm, whereas the size of the glass spheres (packing material) was 4–5 mm (this finding is in agreement with the model of Payatakes, 1973). Chidaglia et al. used large particles and grains in order to have visualization of the filtration process. However, it must be noted that deep-bed filtration is usually employed to remove particles smaller than 50 μm, at a concentration below 500 ppm (Payatakes, 1973; Tien, 1989), whereas the size of the pore constriction in a typical granular filter varies in the range of 20 to 400 μm (Payatakes et al., 1973; Yoshida and Tien, 1985).

The simulator proposed in the present work uses a fully 3-dimensional (3-D) network of unit cells of the constricted-tube-type to represent the void space of the filter, and a 3-D trajectory analysis to calculate the transport and local rates of deposition of non-Brownian particles, along the line of work proposed by Paraskeva et al. (1991) and Burganos et al. (1992a, 1993, 1994, 1995). These concepts are combined with the concepts of deposit morphology and pore clogging, as proposed in Payatakes et al. (1981), suitably modified to apply to 3-D pore networks. The simulator involves four main new features. First, it takes into account the reentrainment of particle clusters when they are exposed to shear stress larger than a critical value, and their redeposition at suitably determined downstream sites. Second, it takes into account the finite permeability of the particle clusters that clog narrow pores, a factor that has *profound* consequences on the dynamic behavior of the system (such as the formation and growth of ''pendants'' and ''pouches''), as reported by Payatakes et al. (1981). Third, redeposition of reentrained clus-

ters can also occur in already clogged pores, causing compounded plug growth. Finally, the algorithm includes the concept of self-clogging of pores, caused by the eventual elimination of the passage along the pore axis at advanced stages of particle deposition. Thus, a relatively simple, yet realistic simulator of the transient behavior of the actual process is obtained. Simulation of the effects of particle deposits on the rate of deposition and the permeability are also included in the present simulator.

Description of the Simulator

The porous medium is represented as a cubic lattice of unit cells of the constricted-tube type, as detailed in Burganos et al. (1992a, 1995). In the present work, the macroscopic pressure gradient is applied in the direction that forms equal angles (φ) with the three principal axes, so as not to favor flow along any of the main directions (Figure 1). Chamber diameter and throat diameter values are assigned to the nodes and branches of the network, respectively, by random chamber and throat-size distributions (CSD and TSD), obtained experimentally (Tsakiroglou and Payatakes, 1990, 1991). The ith unit cell has two mouth diameters, D_{i1} and D_{i2}, which are set equal to the chamber diameters assigned to the corresponding nodes, and a constriction diameter, d_i, which is set equal to the throat diameter assigned to the ith branch. The length of each unit cell is set equal to l. The shape and size of the ith unit cell are uniquely defined by D_{i1}, D_{i2}, d_i and l, and by the assumption that the two parts on either side of the constriction are sinusoidal (axisymmetric cell), and of equal length ($l/2$). In general $D_{i1} \neq D_{i2}$, and so the unit cells are asymmetric with respect to their constriction. The initial porosity, ϵ_0, of the filter is easily matched by adjusting the unit-cell length. The simulation proceeds in a sequence of steps, as described below.

Step 1. The flow field in each unit cell, as generated by the application of a macroscopic pressure gradient, is calculated with the standard network analysis (see, for instance, Constantinides and Payatakes, 1989). The hydraulic conductance of each unit cell is calculated with the collocation method of Tilton and Payatakes (1984), suitably modified for asymmetric unit cells. The initial pressure gradient, ∇P, is chosen so as to yield the desired superficial velocity, $\boldsymbol{\nu}_s$ (that is, flow rate per unit cross-sectional area). This is straightforward because, under creeping flow conditions, ∇P and $\boldsymbol{\nu}_s$ are directly proportional to each other.

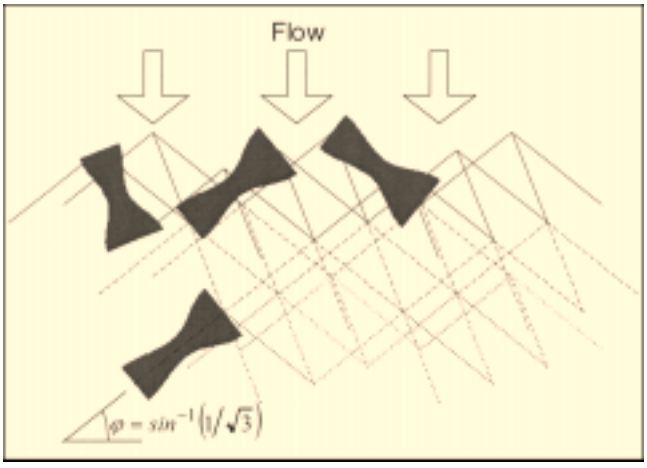

Figure 1. Sample of cubic network of unit cells of the constricted-tube type.

The macroscopic gradient forms equal angles with the three principal directions of the network.

Step 2. The rate of particle deposition in each unit cell is determined with the 3-D trajectory method of Paraskeva et al. (1991). The determination of the overall impacted fraction in a pore is facilitated considerably by the computation of limiting capture trajectories, that is, of particle trajectories that lead to capture at the exit mouth of the pore. Representative limiting trajectories in an inclined pore are shown in Figure 2a. The particle trajectory method can also give the local rate of deposition along the pore walls, which is needed to determine the shape of the deposit in each unit cell. To save computational time, the fraction deposited up to position z^*, $\eta_i(z^*)$, is calculated at three different positions ($z^* = 1/3, 1/2, 1$) along each unit cell (Figure 2b), and an interpolating polynomial is used for intermediate positions.

Step 3. Assuming that the rates of deposition remain constant during a suitably small time interval, δt, the volume of deposited matter in each unit cell during this time interval is readily determined from critical trajectory calculations, assuming that the deposits have a mean porosity ϵ_d. The value of ϵ_d can be experimentally determined, or based on independent particle trajectory ("ballistic") calculations at a sufficiently small scale. Typical values range from ~ 0.6 to ~ 0.8 (Tien et al., 1979; Jung and Tien, 1993; Choo and Tien, 1995a,b). The shape of the deposit in each unit cell is determined as follows. It is assumed that the axial symmetry of the unit cell is retained and that the thickness of the deposited layer at each of the three locations ($z^* = 1/3, 1/2, 1$) is proportional to the local value of $d\eta_i(z^*)/dz^*$ (Figure 3a). The resulting three equations are solved for the three parameters that define the new sinusoidal surface.

Step 4. The flow field in each unit cell at the end of the previous time interval is calculated anew, taking into account the modified shapes of the unit cells, while keeping the superficial velocity, $\boldsymbol{\nu}_s$, constant by increasing ∇P suitably. Note that ∇P and $\boldsymbol{\nu}_s$ remain proportional to each other over the entire filtration cycle studied here. The filtration mode that is simulated here is that of constant flow rate and increasing pressure drop. The mode of constant pressure drop and decreasing flow rate can also be simulated with the same method, by making self-evident changes in the procedure.

Step 5. The shear stress at the constriction in each unit cell is calculated and compared to the preset critical value for reentrainment, π_{cr}. This is a parameter of crucial importance for the dynamic behavior of depth filtration and depends strongly on the particle-to-wall and particle-to-particle adhesiveness. If $\pi_j \geq \pi_{cr}$ in the jth unit cell, then Step 6 must be executed for this unit cell (and in any other similar case) before proceeding any further. This phenomenon occurs at relatively advanced stages of deposition. Otherwise, the simulation skips to Step 8 directly (see below).

Step 6. All the deposited matter in unit cell j is assumed to be reentrained and leave the cell, given that the criterion $\pi_j \geq \pi_{cr}$ is met. The reentrained matter has a known volume

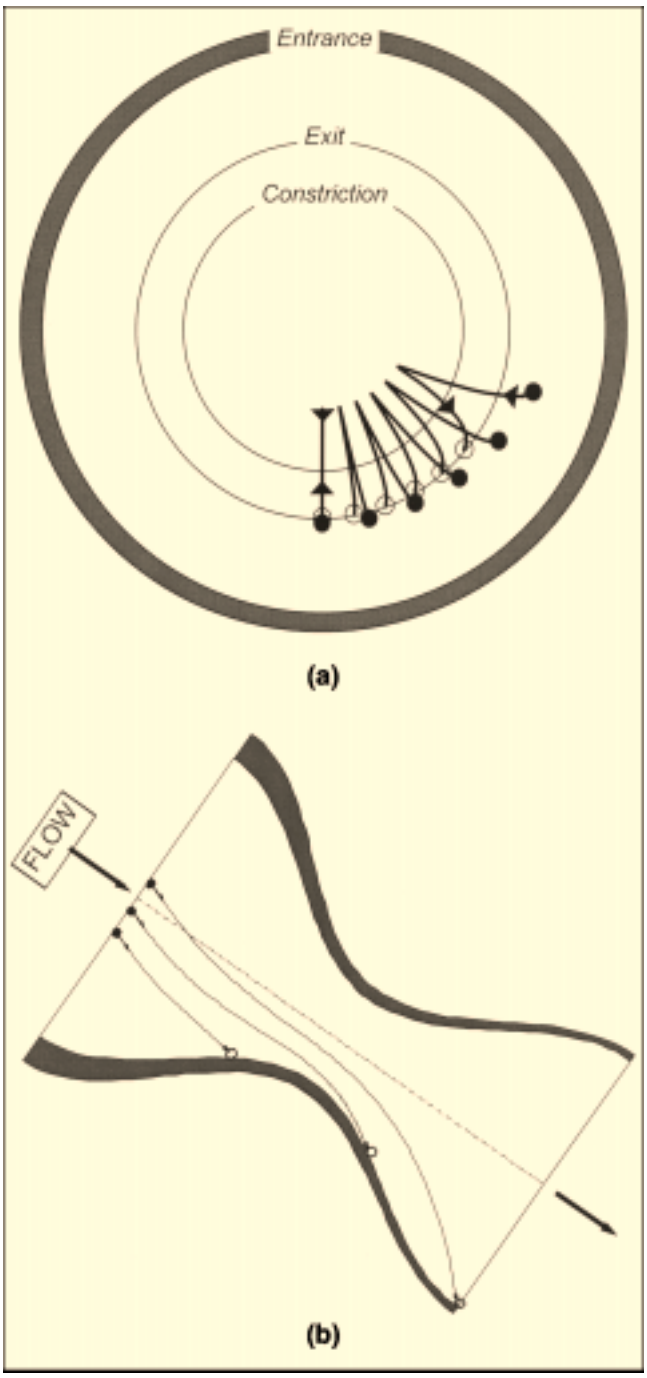

Figure 2. (a) Limiting capture trajectories in a constricted pore with a deposit layer already formed; (b) representative capture trajectories, used to calculate the local deposition rate within a pore and geometry of the layer formed.

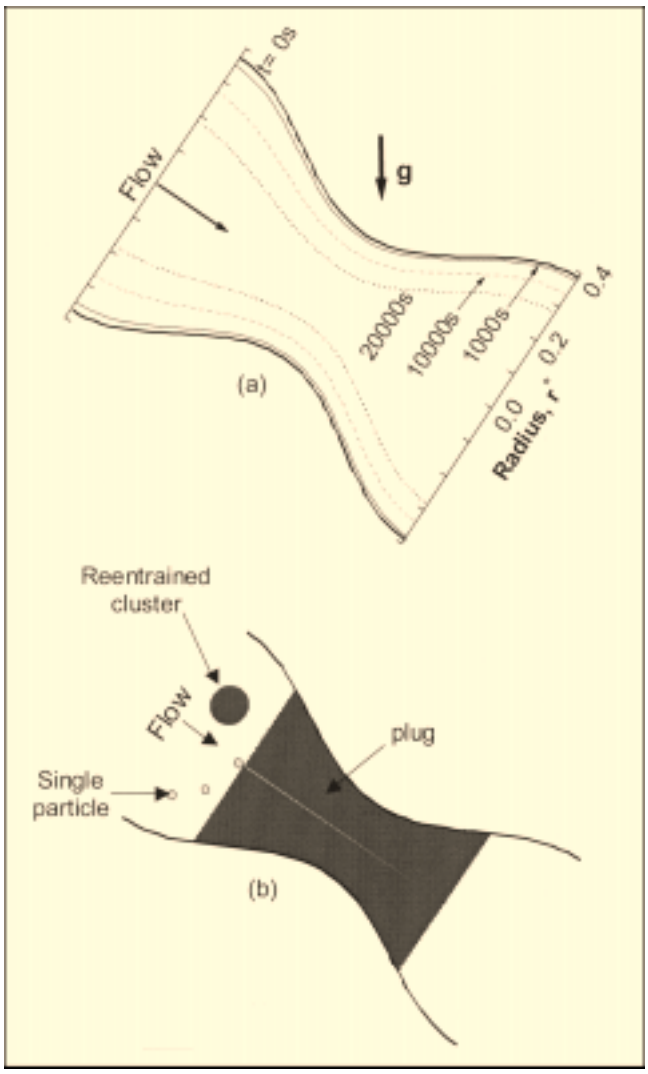

Figure 3. (a) Formation of particle deposits and temporal evolution of the deposit in a constricted pore; (b) idealized plug-type clogging of a pore by a reentrained cluster.

that corresponds to a certain volumetric diameter, say, d_{rm}. This large cluster is assumed to move ''instantly'' downstream, selecting its path at every node that it encounters with probabilities that are proportional to the mass flow rates through the corresponding downstream unit cells, until it reaches a constriction that is narrower than d_{rm}, where it deposits and forms a clog. To simplify the calculation, this clog is assumed to take a pluglike shape of the same volume (Figure 3b). The hydraulic conductance of the ''plug'' is estimated using the Blake-Kozeny (alternatively, the Ergun) equation, and it replaces the conductance that the clogged unit cell had prior to clogging. The new conductance is usually two, or more, orders of magnitude smaller and will reduce the flow rate through the clogged unit cell accordingly. Despite this, the role of a clogged unit cell is significant, because virtually every suspended particle that attempts to pass through it is captured. Thus, ''plugs'' keep growing with significant rates, as reported in Payatakes et al. (1981). Furthermore, redeposition of reentrained clusters can also occur in already clogged pores, causing compounded plug growth.

Step 7. Gradual clogging of pores is caused by progressive thickening of the particle-deposit layer and eventual elimination of the through passages along the pore axis at advanced

stages of particle deposition. This phenomenon is favored when the critical shear stress for reentrainment, π_{cr}, is relatively large, so that the condition for cluster detachment and pore-plugging phenomena is not easily met.

Step 8. Network-averaged local quantities, in particular the specific deposit, σ, the overall filter coefficient, λ, and the pressure gradient, ∇P, are calculated and recorded, as time is updated and the simulator continues with Step 2 (unless otherwise specified) and subsequent steps. Once a layer of deposited material is formed, it is expected that the particle–surface interactions will not be identical to those in clean pores. As mentioned earlier, deposits produce a collector surface that has significant porosity and, consequently, exerts a considerably weaker drag force on the traveling particles, compared to the case of the clean collector surface. For this reason, the hydrodynamic interactions are estimated using the drag-force correction factors evaluated by Michalopoulou et al. (1992, 1993) and Burganos et al. (1992b). In addition, the pore surface potential value, ψ_{02}, which enters the calculation of the electrokinetic (double-layer) force, acquires a new value when deposit is formed. The accurate calculation of this value would be a formidable task in itself. However, Burganos et al. (1993) showed that the impact fraction in a constricted pore is insensitive to the precise value of ψ_{02}, provided that it is lower than a threshold value. Under the conditions of the simulations reported here, this threshold value is -17 mV, whereas the corresponding value for the solid wall is -8 mV and for the suspended particle, -30 mV. Given that the deposits are highly porous, it is estimated that the actual value for the deposits is well below the aforementioned threshold value and, hence, the electrokinetic force calculations are not practically changing with the progress of the filtration process.

Figure 4 shows the structure diagram of the proposed simulator.

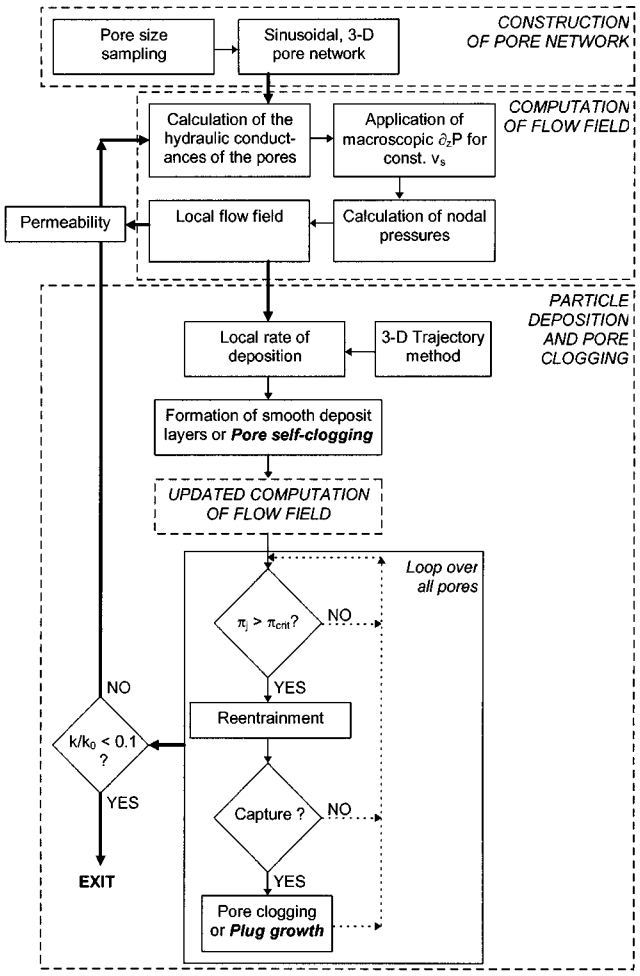

Figure 4. Structure of the simulator.

Results and Discussion

Sample simulation results are given in Figures 5–16 for the specific deposit profiles, the overall filter coefficient λ, the modulating filter coefficient f_λ, the pressure gradient, f_p [$= (\partial_z P)/(\partial_z P)_0$], and the reduced permeability, k/k_0, as functions of the normalized specific deposit, σ/ϵ_0. The simulations were done using a sample network with dimensions ($24 \times 24 \times 150$) and the parameter values given in Table 1. These values were used in previous works (Payatakes, 1973; Payatakes et al., 1974; Rajagopalan et al., 1976; Vaidyanathan and Tien, 1989, 1991; Paraskeva et al., 1991; Burganos et al., 1992), and they are used in the present work for reasons of comparison. All these values are typical values valid for the filtration of a typical stable suspension through a depth filter. The superficial velocity, v_s, the particle diameter, d_p, the critical shear stress, π_{cr}, and the porosity of the deposits, ϵ_d, were changed over ranges of practical interest in order to study their effects on the aforementioned calculations. The values used in each case are given in the corresponding figures.

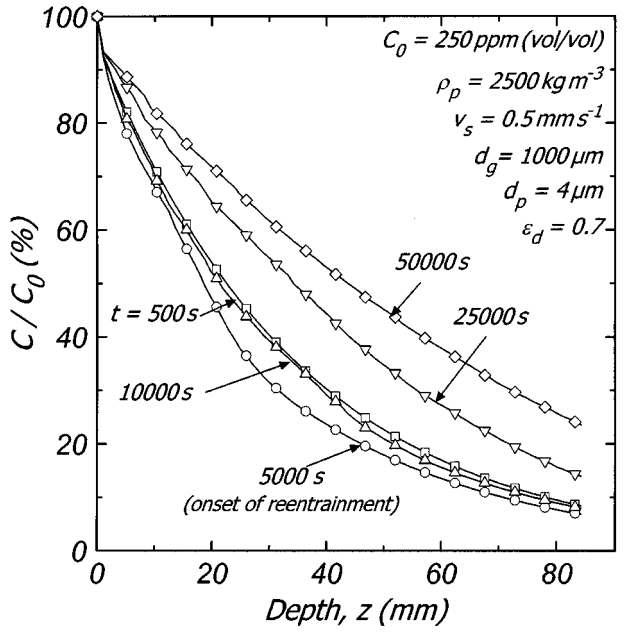

Figure 5. Variation of concentration profiles in the mean flow direction with time.

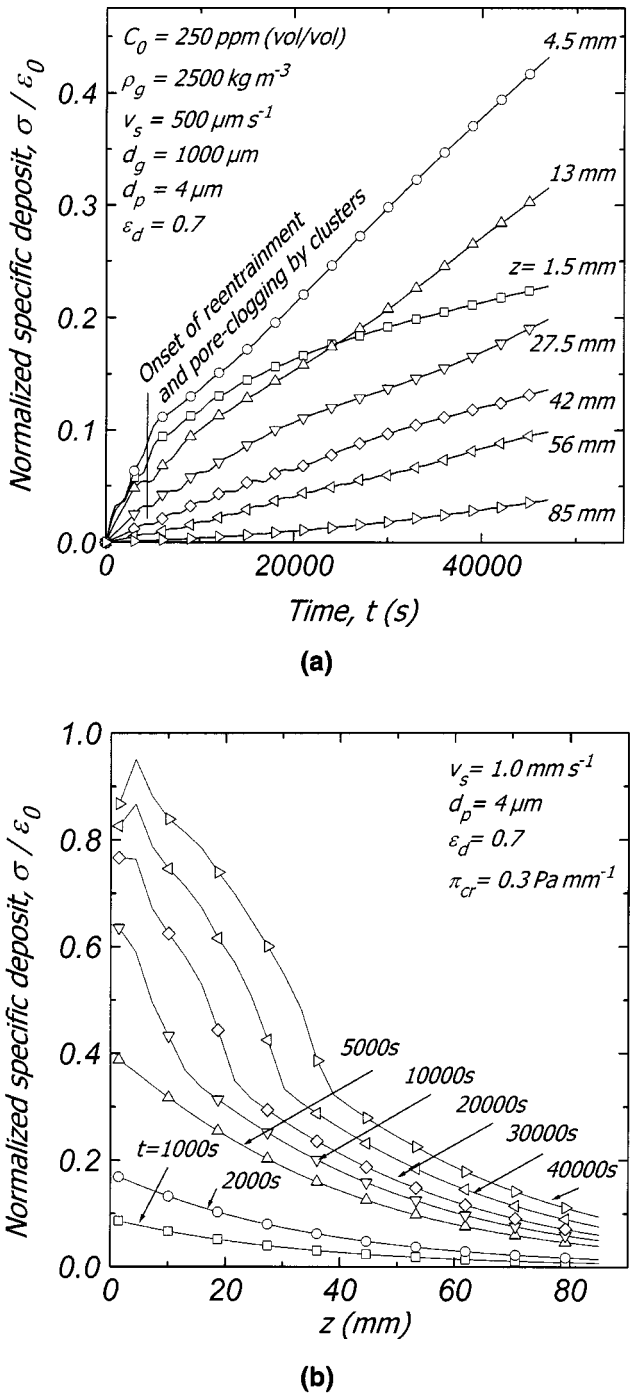

Figure 6. Normalized specific deposit vs.: (a) time at various depth values in the filter; (b) depth (variation with time).

To facilitate the discussion of the results, the observed phenomena of particle deposition, reentrainment of clusters, and pore clogging can be summarized as follows:

P1. Formation of deposited layers by deposition of individual particles on the walls of (unplugged) pores.

P2. Reentrainment of clusters from pores in which the shear stress on the pore constriction exceeds a critical value, π_{cr}.

Table 1. Parameter Values Used in the Simulations

Porous medium parameters
Chamber-size distribution: lognormal, $\mu_g = 800$ μm, $\sigma_g = 66$ μm
Throat-size distribution: lognormal, $\mu_g = 400$ μm, $\sigma_g = 32$ μm
Initial porosity of porous medium, $\epsilon_0 = 0.425$
Unit-cell length, $l = 1{,}000$ μm
Thickness of a five-unit-cell zone, $\Delta z = 2.886$ mm
Cell inclination, $\varphi = \sin^{-1}(1/\sqrt{3}) \approx 35°14'$
Suspension parameters
Monodispersed feed
Particle entrance concentration, $C_0 = 250$ ppm (vol/vol)
Particle diameter, $d_p = 4$ or 10 μm
Particle density, $\rho_p = 2{,}500$ kg·m^{-3}
Water density, $\rho_w = 997$ kg·m^{-3}
Water viscosity, $\mu_w = 0.89$ mPa·s
Dielectric constant of liquid medium, $\tilde{\epsilon} = 81$
Double-layer reciprocal thickness, $\kappa = 2.8 \times 10^8$ m^{-1}
Interaction parameters
Surface potential of suspended particle and pore walls, $\psi_{01} = -30$ mV, $\psi_{02} = -8$ mV, respectively
Hamaker constant, $H = 5 \times 10^{-20}$ J
Externally imposed parameters
Axial-flow mode
Superficial velocity, $v_s = 1.00$, 1.25 or 1.50 mm·s^{-1}
Constant flow rate (increasing macroscopic pressure gradient)
Adjustable parameters
Porosity of deposit, $\epsilon_d = 0.7$ or 0.8
Critical shear stress, $\pi_{cr} = 0.3$ or 1.0 Pa

P3. Pore clogging by a cluster with volumetric diameter greater than that of the corresponding pore constriction (sudden pore clogging).

P4. Plug growth in clogged pores by capture of individual particles and/or oncoming clusters.

P5. Deposited layer rearrangement to form a plug-shaped clog in the *same* pore, when the open pore constriction becomes comparable to the individual particle size (gradual pore clogging).

Figure 5 shows the dependence of the concentration ratio, C_{eff}/C_0, on the depth in the filter at various filtration stages. As expected, the effluent concentration, C_{eff}, decreases with depth, which is also in accord with experimental data (Ives, 1961; Ison and Ives, 1969; Tien et al., 1979; Tien, 1989). It is interesting to observe that the concentration profiles display mixed behavior, as discussed in Tien and Payatakes (1979) and Tien (1989). This remarkable behavior is explained below, in connection with the dependence of the filter coefficient λ on the specific deposit σ.

Figure 6a shows the temporal evolution of the normalized specific deposit, σ/ϵ_0, at various depths in the filter. The specific deposit, σ, is defined as the volume of the material deposited within a layer of thickness Δz divided by the total volume of this layer, whereas ϵ_0 is the initial filter porosity. In order to obtain space-averaged results, an average was taken over a zone with thickness of five unit cells along the mean flow direction. A large portion of deposited material is found at small depths and the amount increases monotonically with time. Deeper parts of the filter contribute less to the removal of suspended particles, in accord with experimental data (Ives, 1961; Ison and Ives, 1969; Tien et al., 1979; Tien, 1989). The rate of particle deposit growth in the first zone, $z = 1.5$ mm, appears to decrease after $\sim 5{,}000$ s be-

cause of the detachment of particle clusters from the walls and reentrainment into the main stream. During their migration downstream, reentrained clusters may clog narrow pores that they encounter. Figure 6b shows the variation of the normalized specific deposit along the filter, at different times. In general, the specific deposit decreases with depth. It is also noteworthy that deposition takes place mainly within the upper part of the filter, whereas the lower part of the filter appears to contribute to filtration only at very advanced stages of filtration, in full accord with experimental results (Tien and Payatakes, 1979; Tien, 1989).

The filter coefficient, λ, which is the parameter that characterizes the local effectiveness of the depth filter, is calculated from the expression

$$\left(\frac{\partial C}{\partial z'}\right)_{\tau} = -\lambda C \tag{1}$$

(Ives, 1960), where z' is the axial coordinate of the bed (depth), τ is time, and C is the average concentration at z' and τ. In the case of clean filters (that is, during the initial stages of filtration), one can assume that C is not a function of z' and integrate Eq. 1 directly. Thus, a simple expression for the clean filter coefficient, λ_0, is obtained, namely,

$$\lambda_0 = -\frac{1}{L}\ln\frac{C_{\text{eff}}}{C_0} \tag{2}$$

where L is the total length of the filter, C_{eff} is the effluent stream concentration, and C_0 is the feed concentration.

Since particle deposition alters the geometry of the void space within the filter, the distribution of the deposited material within the filter varies with depth and time and, consequently, Eq. 1 can no longer be directly integrated along the filter. To overcome this problem, the overall filter coefficient can be expressed as

$$\lambda = \lambda_0 f_\lambda(\sigma, \boldsymbol{\alpha}), \tag{3}$$

where f_λ is a correcting factor that accounts for the deviation from the logarithmic dependence (Tien and Payatakes, 1979; Tien, 1989) of the collection efficiency on the effluent concentration, and $\boldsymbol{\alpha}$ is a vector of system parameters. Various empirical forms have been suggested for f_λ in the literature (see Tien, 1989, for a synopsis of such expressions). Clearly, f_λ depends on each and every parameter that affects particle deposition within the filter, for example, parameters that enter the calculation of the local particle deposition rate, the morphology of deposits and their distribution within the filter, the filtration velocity, the particle- and grain-size distributions, and the magnitude of surface and hydrodynamic interactions. All proposed empirical expressions include adjustable parameters, the values of which are determined by fitting experimental data. Such parameter values apply strictly to the particular system under consideration and do not provide insight into the phenomena that underlie the system behavior. On the other hand, true-to-mechanism simulators, such as the one developed here, are designed to predict the dependence of λ_0 and f_λ on all the system parameters and to provide insight into the various aspects of the dynamic behavior of the process.

Below, we present simulation results for the profiles of f_λ and λ, in the form of space-averaged values, by averaging their local values over zones containing five sequential layers of cells, which defines the zone thickness as ~ 3 mm. The concentration in each zone is assumed to be constant, so that Eq. 2 can be employed for the calculation of λ and f_λ:

$$\lambda_{z'} = -\frac{1}{\Delta z}\ln\frac{C_{\text{eff},z'}}{C_{0,z'}}, \tag{4}$$

where Δz is the thickness of the zone, $C_{\text{eff},z'}$ is the effluent concentration, and $C_{0,z'}$ is the feed concentration in the zone under consideration. The $f_{\lambda,z'}$ values shown in the figures are calculated as the ratio $\lambda_{z'}/\lambda_0$, where λ_0 is the clean filter coefficient. For the sake of simplicity, $f_{\lambda,z'}$ and $\lambda_{z'}$ are also noted as f_λ and λ, and referred to as filter coefficient modulating function and filtration coefficient, respectively, in the discussion of the figures.

Figure 7 shows the variation of the filter coefficient modulating function with the normalized specific deposit at different depths into the filter. The effect of the superficial velocity on this variation is also shown in the figure. Three main regions can be identified in each case. The first region is associated with rather smooth deposition along the pore walls (phenomenon P1), and hence for small values of σ/ϵ_0, the dependence of f_λ on σ/ϵ_0, is weak. In this region f_λ decreases slightly with increasing σ. This is explained by the fact that the growing smooth deposits cause an increase in the local interstitial velocity (given that the flow rate is constant), which in turn causes a slight decrease in the rate of deposition (Paraskeva et al., 1991; Burganos et al., 1992a). This observation applies to all depths and superficial velocity values examined in this figure. A relatively abrupt increase in the value of f_λ is observed as a critical σ/ϵ_0 value is reached (region 2). This sharp change is attributed to the detachment of whole particle clusters from the pore walls and their transport downstream, where they clog narrow pores within the same or adjacent zones (phenomena P2 and P3). Clogged pores act as additional collectors with the maximum collecting efficiency, since any individual particle and/or oncoming cluster is destined to entrapment within the porous plug (phenomenon P4). The flow in region 3 takes place through the relatively few unplugged pores at high velocity, where much slower deposition takes place (Paraskeva et al., 1991; Burganos et al., 1992a), while the phenomenon of plug growth in clogged pores (phenomenon P4) is still active. Reentrainment of particle clusters and further pore clogging are relatively less frequent than in region 2.

It is important to note that the combined behavior of f_λ vs. σ in regions 1 and 2 is a *new* theoretical prediction that requires careful experimental investigation for possible confirmation. Several investigators have already reported that f_λ increases with σ for small values of σ (for reviews, see Tien and Payatakes, 1979; Tien, 1989), but the existence of region 1 before region 2 has not been reported. This is easy to explain, however, because region 1 is rather narrow and therefore easy to miss, if one is not aware of its possible existence. In typical experiments, the first sampling port *in* the filter is located *beyond* region 1. Furthermore, the form of f_λ vs. σ is obtained indirectly through the fitting of macroscopic concentration profiles, using phenomenological functions that do

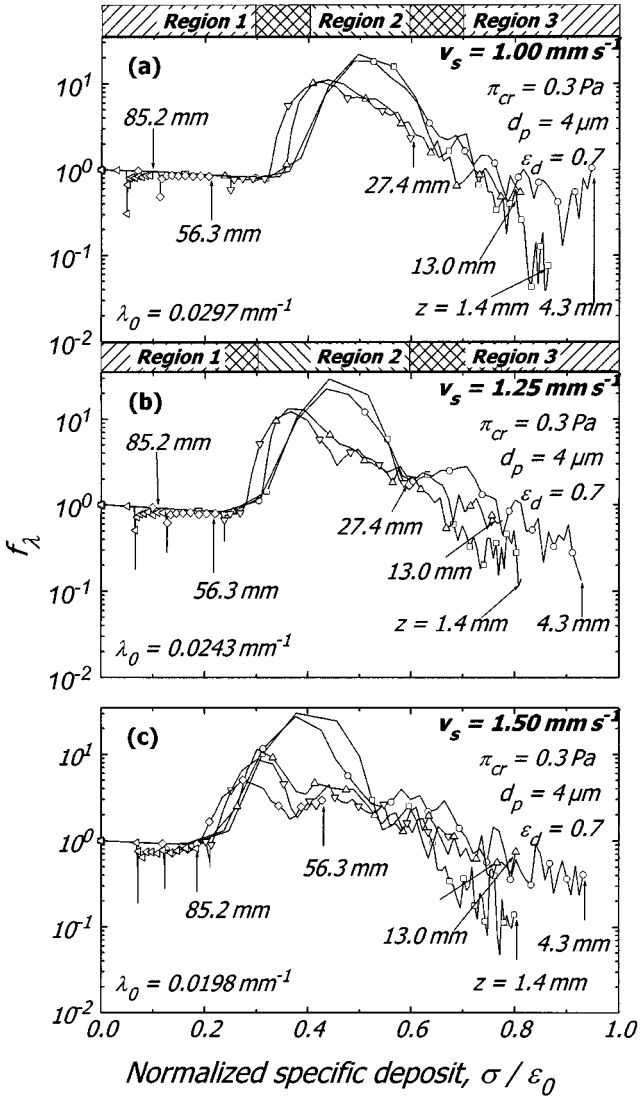

Figure 7. Filtration coefficient modulating function vs. normalized specific deposit at several depth values in the filter.

Effect of the superficial velocity. The arrows denote the end of each curve (also, the end of simulation).

not allow for an inflection point (such as the one that occurs between regions 1 and 2). Careful experimental investigation of this aspect of the progress is warranted.

At the lower part of the filter (for example, $z = 56.3$ mm or 85.2 mm in Figure 7), deposition takes place only in the form of relatively uniform deposition (P1). Catastrophic phenomena, such as cluster reentrainment or pore clogging, are not observed. This is not the case with intermediate depths ($z =$ 13.0 mm or 27.4 mm), where intensive pore clogging may develop, resulting from cluster reentrainment within the upper part of the filter.

The effect of superficial velocity, v_s, on filter performance is discussed next. The initial filter coefficient, λ_0, decreases as v_s increases, in accord with the corresponding predictions of previous work (see, for instance, Tien and Payatakes, 1979; Tien, 1989; Burganos et al., 1992a, 1995). Region 1 shrinks, region 2 shifts left, that is, to lower σ/ϵ_0 values, while maintaining its breadth, and region 3 expands to the left. This means that increasing v_s promotes catastrophic phenomena (P2, P3, P4), chiefly through the increase of the shear stress inside the pores, causing cluster detachment. Therefore, operation at elevated flow rates is seen to reduce the removal efficiency of the filter at smaller values of σ/ϵ_0. Of course, this is not necessarily a drawback, because at large flow rates the throughput increases and larger quantities of the suspension are filtered within the same period of time.

Figure 8 shows the filter coefficient modulating function of *individual particles* with the normalized specific deposit, at different depths in the filter. The f_λ values are calculated by considering only the individual particles that enter into or escape from a certain zone in the evaluation of C_0 and C_{eff}, respectively. The curves of Figure 8 are almost identical to those of Figure 7 for the same v_s value (the curves are slightly shifted to the right in Figure 8), which implies that the calculated values for f_λ in Figure 7 are essentially based on the number of individual particles that enter into or escape from a certain zone. The reentrained clusters of particles do play a significant role in the particle capture process, but they rarely manage to exit from the zone of detachment and, thus, do not affect the calculation of f_λ (or λ) significantly.

The effects of the parameters, π_{cr}, ϵ_d, and d_p on the behavior of particle deposition and pore plugging (in terms of f_λ) are shown in Figures 9a–9c, where all other parameter values are identical to those used in Figure 7a. It is clear that increasing the π_{cr} value (to 1 Pa) results in the broadening of region 1 (Figure 9a). The reason is that thick deposits are allowed to grow by the increased level of critical shear stress that must be reached for detachment and reentrainment to occur. At $z = 27.4$ mm or further downstream, deposition proceeds in a smooth fashion and progresses without any detachment phenomena. When the critical shear stress is reached, the reentrained clusters are large and tend to plug pores that are encountered downstream within the same zone. The collection efficiency in region 3 increases as π_{cr} in-

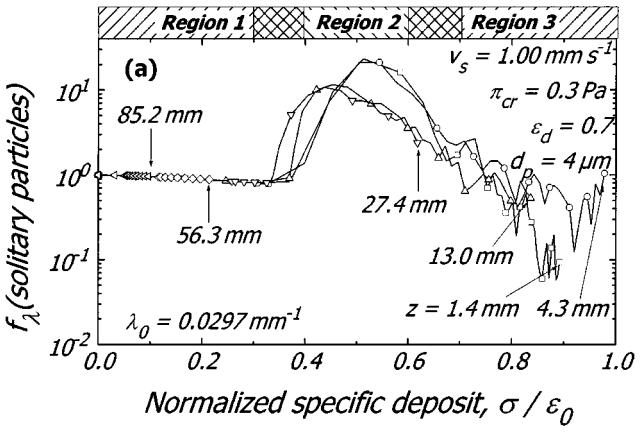

Figure 8. Filtration coefficient modulating function for individual particles vs. normalized specific deposit at several depth values in the filter.

Effect of the superficial velocity. The arrows denote the end of each curve (also, the end of simulation).

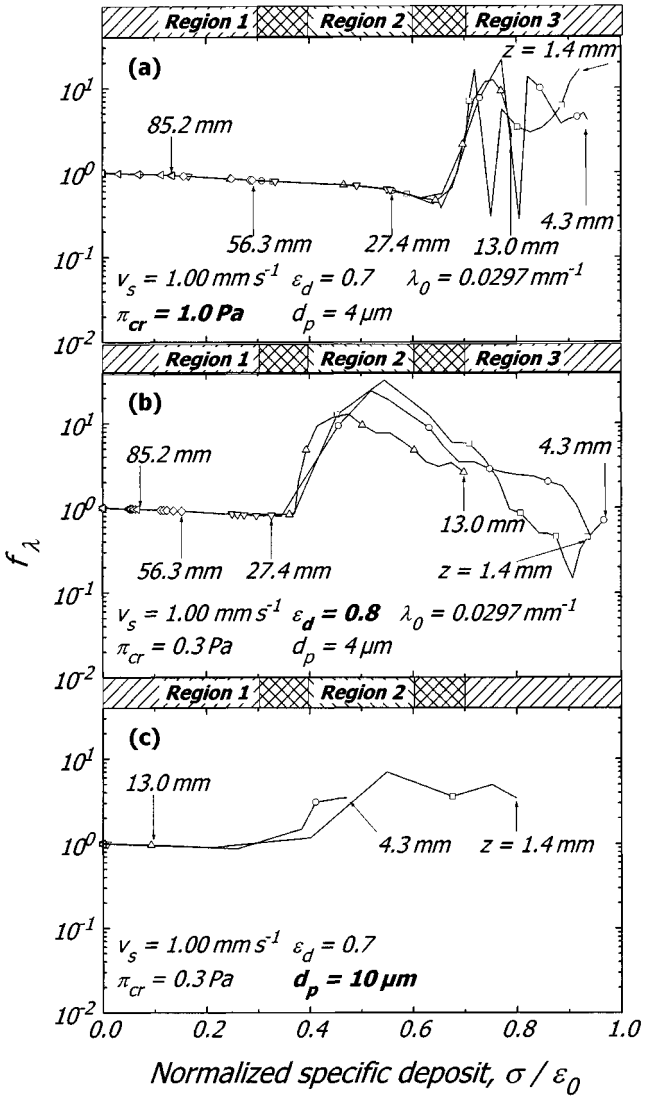

Figure 9. Filtration coefficient modulation function for individual particles vs. normalized specific deposit at various depths.

Effects of (a) critical shear stress, (b) porosity of deposition, and (c) particle diameter. The arrows denote the end of each curve (also, the end of simulation).

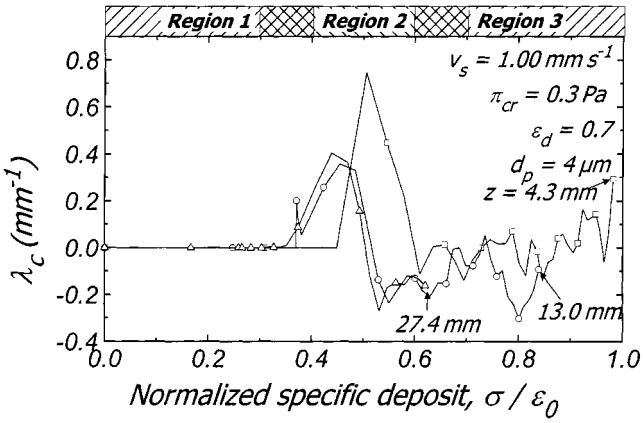

Figure 10. Cluster filtration coefficient vs. normalized specific deposit at various depths.

The arrows denote the end of each curve (also, the end of simulation).

creases, and remains large even at very large values of the specific deposit ($\sigma/\epsilon_0 = 0.8$).

An increase in the porosity of the deposits from 0.7 to 0.8 leaves region 1 practically unchanged (compare Figures 9b and 7a). Also, the pore-clogging phenomena begin at the same specific deposit value. However, the overall process in the higher deposit porosity case completes the same stages in about half the time that is needed in the case of lower porosity (see, for instance, depth $z = 27.4$ mm for comparison). Since the porosity of the deposits is greater, reentrained clusters are of larger volume and become trapped mainly in the upper part of the network. Finally, increase in the particle size in the suspension (Figure 9c) gives rise to a behavior that resembles the case of cake filtration, where the phenomena of particle deposition and pore clogging take place mainly in the upper part of the filter, the lower part remaining almost unutilized over the entire filtration process.

Figure 10 shows the variation of the cluster filtration coefficient, λ_c, with the normalized specific deposit. The calculation of λ_c is made in a manner similar to that used for λ; the only difference is that C_0 and C_{eff} in Eq. 2 refer to the cluster concentrations at the entrance and exit, respectively, of the zone under consideration. Some of the clusters that enter a specific zone are trapped, whereas the rest move to the next downstream zone. Within a single zone, formation of new clusters may occur, possibly followed by reentrainment and entrapment within the same zone, or escape to the next zone. At low values of σ/ϵ_0, cluster activity is not likely to develop. At advanced filtration stages ($\sigma/\epsilon_0 > 0.4$ in Figure 10), the rate of cluster efflux from a certain zone is lower than the rate of cluster influx into the zone ($C_{\text{eff}} < C_0$). At very high values of σ/ϵ_0 (> 0.7 in Figure 10), the inverse phenomenon is observed, namely, the rate of cluster efflux from a certain zone is higher than that of cluster influx into the zone ($C_{\text{eff}} > C_0$). However, it must be noted that the number of particles that compose the moving clusters in a certain zone is, under typical operating conditions, one order of magnitude smaller than the number of individual particles that travel within the zone in the same period of time.

The variation of the filtration coefficient for individual particles, λ_s, and of the cluster filtration coefficient, λ_c, with time, is shown at different depths in Figure 11a and 11b, respectively. Figure 11a shows that the filter is initially most active in the upper zones ($z = 3$ mm and 6 mm) and less active in the lower zones ($z = 15$ mm and 30 mm). Following an initial increase, λ_s declines with time in a given zone, owing to the progressive narrowing of the pore constrictions, which gives rise to increased suspension velocities and, consequently, to reduced deposition rates. Figure 11b shows that the catastrophic phenomena take place during the entire period of filter operation sustaining cluster activity, except for the very early stages of simulation ($t < 5000$ s).

The pressure gradient in the mean flow direction changes with time and depends strongly on the pattern of deposition

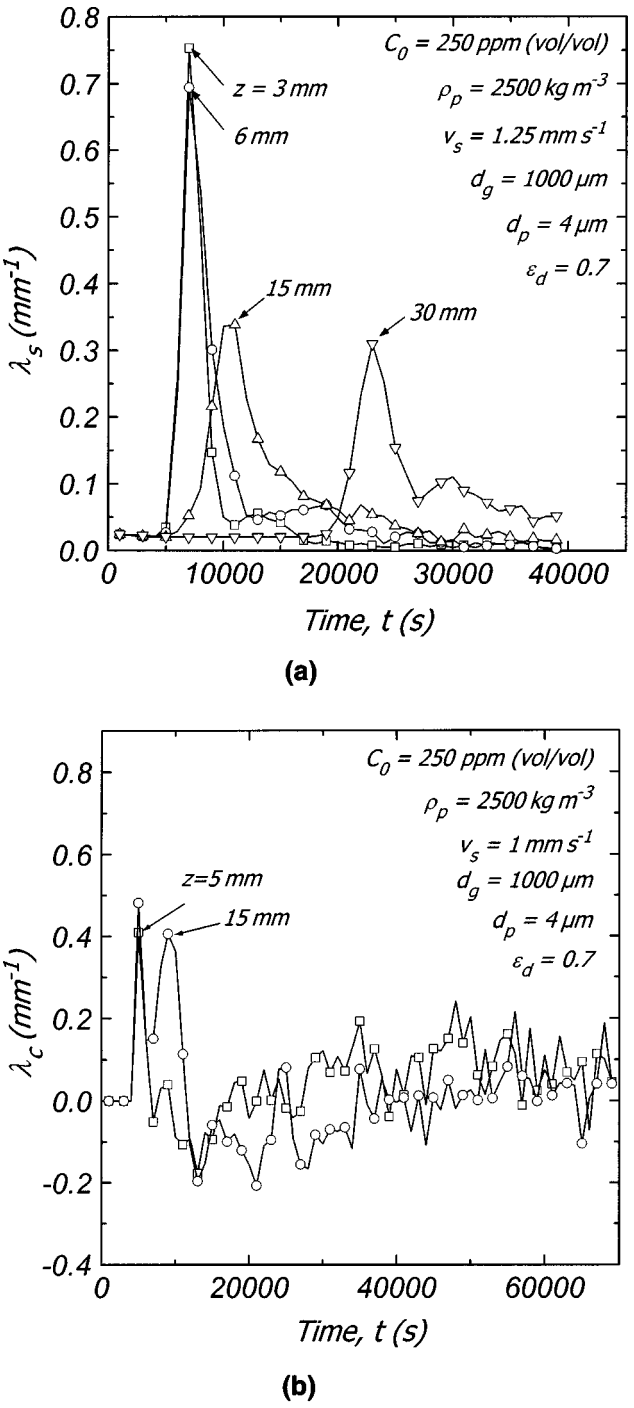

Figure 11. Temporal evolution of filtration coefficient: (a) for individual particles, λ_s; (b) for clusters, λ_c, at various depths.

within the filter. The following expression is usually used:

$$\left(\frac{\partial P}{\partial z'}\right)_{\tau} = f_p(\sigma, a)\left(\frac{\partial P}{\partial z}\right)_0, \tag{5}$$

where $(\partial P/\partial z)_0$ is the magnitude of the pressure gradient at startup, and f_p is a correction factor that depends on the

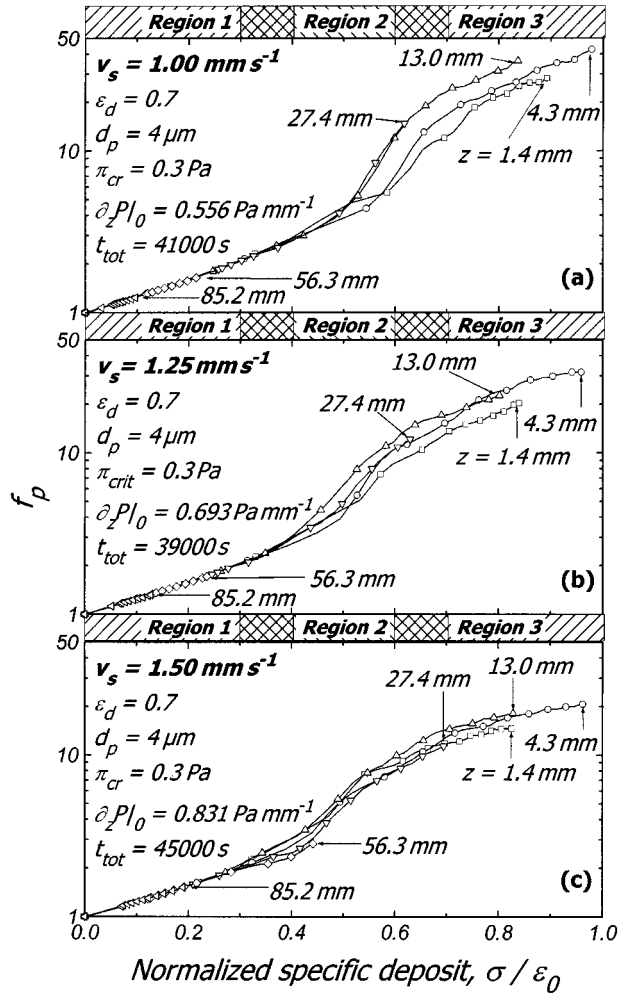

Figure 12. Variation of the magnitude of the reduced pressure gradient, f_P, with the normalized specific deposit at various depths.

Effect of the superficial velocity. The arrows denote the end of each curve (also, the end of simulation).

same parameters as those affecting f_λ (see earlier). Empirical expressions for f_p are summarized in Tien (1989) and include adjustable parameters, the determination of which requires a series of filtration experiments in pilot plants. Equation 5 can also be expressed in terms of the permeability as follows:

$$k = k_0/f_p(\sigma, a), \tag{6}$$

where k is the permeability at a given porosity and time, whereas k_0 is the permeability of the clean filter.

Figure 12 shows the dependence of the reduced pressure gradient, $f_p = (\partial_z P)/(\partial_z P)_0$, and therefore of the inverse of the reduced permeability on the normalized specific deposit. Three different values are used for the magnitude of the superficial velocity, v_s (Figures 12a–12c). Again, three distinct regions can be identified in each graph. In the first region, that is, for small values of σ/ϵ_0, a nearly linear increase of $(\partial_z P)/(\partial_z P)_0$ is observed, caused by the formation of smooth

deposits in relatively open pores (P1). The slope of the curves in this region is invariant with depth and superficial velocity, exactly as it was observed in Figure 7 for f_λ. As σ/ϵ_0 increases, a sharper increase on $(\partial_z P)/(\partial_z P)_0$ is observed (region 2), because of the plugging of pores by reentrained clusters (P2, P3). The hydraulic conductances of plugged pores are usually two or more orders of magnitude smaller than those of open pores. As deposition continues, the rate of increase of $(\partial_z P)/(\partial_z P)_0$ becomes smaller again (region 3), because the local interstitial velocity increases so that further local deposition diminishes. Cluster reentrainment and pore clogging begin at smaller values of σ/ϵ_0 as the superficial velocity increases (compare Figures 12b and 12c), because of the increase in the local shear stress. This leads to the formation of clusters of smaller volume, which tend to migrate deeper into the filter (Figure 12c).

The effects of π_{cr}, ϵ_d, and d_p on the behavior of particle deposition and pore clogging are quantified in Figure 13 through the reduced pressure gradient, f_p. Comparison of Figures 13a–13c should be made with Figure 11a, where all other data (apart from π_{cr}, ϵ_d, and d_p) are identical. The increase in the critical shear-stress value causes a widening of the region of nearly linear increase of the reduced pressure gradient with the reduced specific deposit, extending over the range 0–0.7. Thick layers of deposits are formed, because the high critical shear stress allows for smooth and gradual growth of the particle deposits. The hydraulic resistance of pores with very thick deposits is significant and comparable to that of plugged pores. Thus, a balance between the contribution of cluster reentrainment (increase of the pore hydraulic conductance) and pore clogging (decrease of the pore hydraulic conductance) is established over the plateau of region 2. The outcome of this interplay is an increase in the pressure gradient as the specific deposit increases (region 3), because sudden pore clogging turns out to be the controlling factor, promoted by gradual pore clogging (P5).

The effect of the porosity of the deposits on f_p is shown in Figure 13b. Thick layers are formed on the pore walls and act as additional collectors, thus amplifying particle deposition. The main part of the deposition is observed in the upper part of the network, while cluster reentrainment was observed only at relatively large values of σ/ϵ_0. The increase in the suspended particle size ($d_p = 10\mu$m) results in earlier clogging of the pores in the upper part of the filter (Figure 13c), whereas removal of particles from the main stream is not likely to occur at depths larger than $z = 13$ mm. The particle-size distribution is of great importance when a filtration system is to be designed, and further work of the type presented here is required in order to elucidate its effect on the filter behavior under a variety of operating conditions.

Figure 14 shows the distribution of plugged pores through the filter and its evolution with time. The parameter values used here are the same as those given in Figure 7a. Averages over layers with thickness of 15 unit cells are shown in this figure. At early stages of filtration, pore plugging develops in the upper part of the filter. Later, the phenomenon extends to the intermediate and lower parts, although it remains most intensive in the upper part. It is noteworthy that the number fraction of clogged pores is almost 65% after 11 h of filter operation, even in the intermediate zones of the filter, under the conditions used in the present simulations. At the same

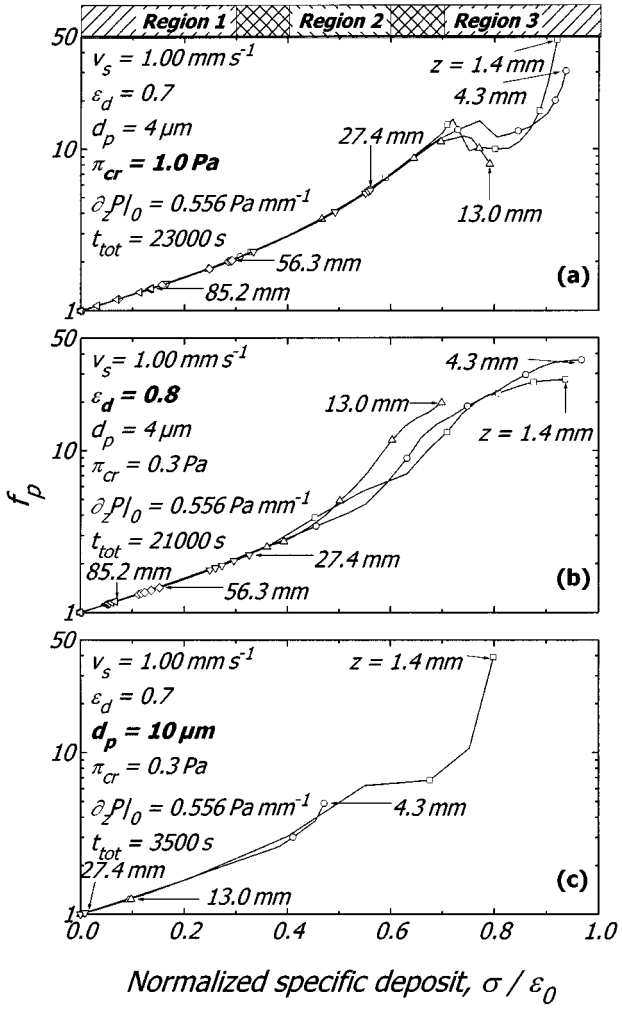

Figure 13. Variation of the magnitude of the reduced pressure gradient, f_P, with the normalized specific deposit at various depths.

Effects of (a) critical shear stress, (b) porosity of deposits, and (c) particle diameter. The arrows denote the end of each curve (also, the end of simulation).

time, the number fraction of clogged pores in the entire filter is approximately 0.2 (Figure 15). Note that during the first 4 h of operation all clogged pores are located within the upper 10% of the filter. At later stages, pore clogging extends to the rest of the filter, in the form of a moving front. This observation is also in accord with experimental observations.

The variation of the filter permeability with the overall specific deposit is shown in Figures 16a–16c. The permeability decreases as the specific deposit increases (Eq. 6). The three aforementioned regions are evident here as well. As the flow rate increases (Figure 16a), cluster reentrainment and pore clogging begin at gradually decreasing values of the specific deposit, because of earlier development of large shear stresses inside the pores. This, in turn, causes smaller clusters to be reentrained, as compared to those under small flow-rate operation, and the probability of pore clogging by reentrained clusters decreases. These phenomena occur over a relatively large filter depth and, consequently, the permeabil-

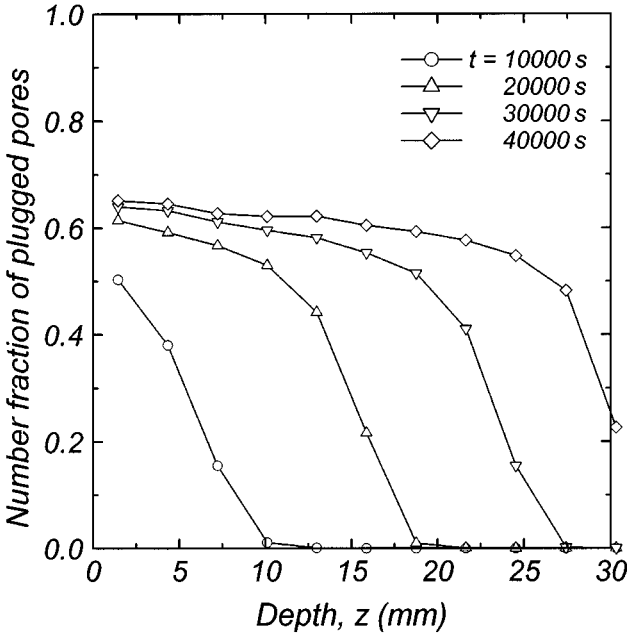

Figure 14. Temporal evolution of the distribution of plugged pores.

Parameter values from Table 1.

ity loss is less pronounced than in the small flow-rate case. The same argument can explain the heavier loss of permeability when the critical shear stress value is decreased (Figure 16b). On the contrary, high critical stress values delay the occurrence of catastrophic phenomena, thus allowing thick

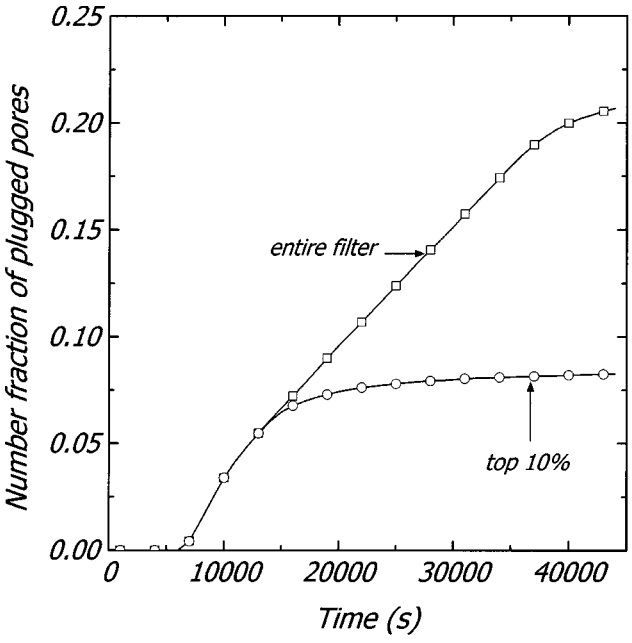

Figure 15. Variation of the number fraction of clogged pores (number of clogged pores divided by total number of pores in the filter) with time.

Contribution of the upper zone of the filter (top 10%). Parameter values from Table 1.

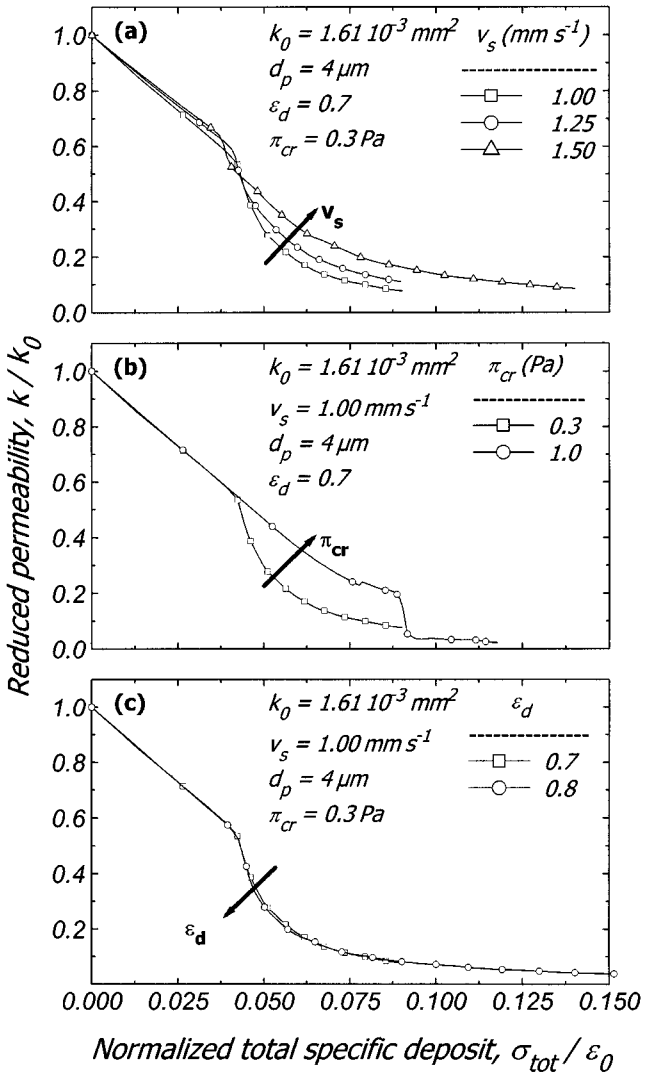

Figure 16. Dimensionless permeability vs. overall normalized specific deposit.

Variation with (a) the superficial velocity, (b) the critical shear stress value, and (c) the porosity of the deposits.

deposits to develop inside the pores. Consequently, for large specific deposit values, relatively large clusters become reentrained and cause rapid clogging of downstream pores and abrupt loss of permeability. Figure 16c indicates that the porosity of the deposits has a negligible effect on the rate of permeability reduction under the conditions assumed here.

Conclusions

A mechanistic simulator of the dynamic behavior of depth filtration of non-Brownian particles was developed. It uses a 3-D pore network and 3-D particle trajectory calculations, and it includes cluster-reentrainment and pore-clogging phenomena, which are responsible for the distinctive macroscopic behavior of the depth filtration systems. The new simulator is used to investigate key phenomena that affect the dynamics of filtration, specifically, formation of gradually growing layers by deposition of individual particles on the pore walls;

reentrainment of clusters from pores, where the shear stress on the pore constriction exceeds a critical value, π_{cr}; pore clogging by a cluster with diameter larger than that of the corresponding pore constriction; and plug growth in clogged pores by entrapment of individual particles and/or oncoming clusters. Rearrangement of deposited layers to form a plug-shaped clog in the *same* pore, when the open pore constriction becomes comparable to individual particle size (pore self-clogging), is also included.

The simulator is capable of determining the effect of the particle deposition pattern on the overall filter efficiency, and the loss of permeability even at advanced stages of filtration. Sample calculations for the overall filter coefficient and the pressure drop show that the simulator can be used to predict effluent concentrations, filter efficiency, and permeability loss as functions of depth and time over a complete filter operation cycle. The role of pore-clogging phenomena was examined for a variety of typical values of the system parameters. It was found that under typical operating conditions pore clogging is more intense in the front layers of the filter and advances in the form of a moving front, deeper in the filter as the process develops. The strong dependence of the filter coefficient on the specific deposit and all the system parameters is predicted in a realistic and satisfactory manner. The value of the critical shear stress for deposit detachment and the suspension flow rate are found to significantly affect the behavior of the filter profoundly, whereas the porosity of the deposits has a rather weak effect. Finally, the filtration efficiency and the loss of permeability are shown to be very sensitive to the size of the suspended particles. The investigation of the transient behavior of granular filters processing polydisperse suspensions is examined in ongoing work.

Acknowledgments

This work was supported financially by the Institute of Chemical Engineering and High Temperature Chemical Processes—Foundation for Research and Technology, Hellas (ICE/HT-FORTH) and by the Commission of the European Union (research grant ERBIC15 CT980911).

Literature Cited

Bai, R., and C. Tien, "A New Correlation for the Initial Filter Coefficient Under Unfavorable Surface Interactions," *J. Colloid Interf. Sci.*, **179**, 631 (1996).

Bai, R., and C. Tien, "Particle Deposition Under Unfavorable Surface Interactions," *J. Colloid Interf. Sci.*, **218**, 488 (1999).

Bai, R., and C. Tien, "Transient Behavior of Particle Deposition in Granular Media Under Various Surface Interactions," *Colloids Surf., A: Physicochem. Eng. Aspects*, **165**, 95 (2000).

Burganos, V. N., C. A. Paraskeva, and A. C. Payatakes, "Three-Dimensional Trajectory Analysis and Network Simulation of Deep Bed Filtration," *J. Colloid Interf. Sci.*, **148**, 167 (1992a).

Burganos, V. N., A. C. Michalopoulou, G. Dassios, and A. C. Payatakes, "Creeping Flow Around and Through a Permeable Sphere Moving with Constant Velocity Towards a Solid Wall: A Revision," *Chem. Eng. Commun.*, **117**, 85 (1992b).

Burganos, V. N., C. A. Paraskeva, and A. C. Payatakes, "Parametric Study of Particle Deposition in Sinusoidal Pores of Arbitrary Orientation," *J. Colloid Interf. Sci.*, **158**, 466 (1993).

Burganos, V. N., C. A. Paraskeva, P. D. Christofides, and A. C. Payatakes, "Motion and Deposition of Non-Brownian Particles in Upflow Collectors," *Sep. Technol.*, **4**, 47 (1994).

Burganos, V. N., C. A. Paraskeva, and A. C. Payatakes, "Monte Carlo Network Simulation of Horizontal, Upflow, and Downflow Depth Filtration," *AIChE J.*, **41**, 272 (1995).

Camp, T. R., "Theory of Water Filtration," *Proc. ASCE, J. Sanit. Eng. Div.*, **90**(SA4), 3 (1964).

Chauveteau, G., L. Nabzar, and J.-P. Coste, "Physics and Modeling of Permeability Damage Induced by Particle Deposition," Int. Symp. on Formation Damage Control, Lafayette, LA (1998).

Chiang, H. W., and C. Tien, "Dynamics of Deep Bed Filtration: I. Analysis of Two Limiting Situations," *AIChE J.*, **31**, 1349 (1985).

Chidaglia, C., L. de Arcangelis, J. Hinch, and E. Guazzelli, "Transition in Particle Capture in Deep Bed Filtration," *Phys. Rev. E*, **53**, R3028 (1996a).

Chidaglia, C., L. de Arcangelis, J. Hinch, and E. Guazzelli, "Hydrodynamic Interactions in Deep Bed Filtration," *Phys. Fluids*, **8**, 6 (1996b).

Choo, C.-U, and C. Tien, "Analysis of Transient Behavior of Deep-Bed Filtration," *J. Colloid Interf. Sci.*, **169**, 13 (1995a).

Choo, C.-U, and C. Tien, "Simulation of Hydrosol Deposition in Granular Media," *AIChE J.*, **41**, 1426 (1995b).

Cleasby, J. L., and E. R. Baumann, "Selection of Optimum Filtration Rates for Sand Filters," *Bull. 198* of the *Iowa State Univ. Bull.*, Vol. LX, No. 34 (1962).

Constantinides, G. N., and A. C. Payatakes, "A Three Dimensional Network of Consolidated Porous Media. Basic Studies," *Chem. Eng. Commun.*, **81**, 55 (1989).

Deb, A. K., "Theory of Sand Filtration," *Proc. ASCE, J. Sanit. Eng. Div.*, **95**, 399 (1969).

Elimelech, M., "Predicting Collision Efficiencies of Colloidal Deposition in Porous Media," *Water Res.*, **26**, 1 (1992).

Elimelech, M., "Particle Deposition on Ideal Collectors from Dilute Flowing Suspension: Mathematical Formulation, Numerical Solution, and Simulation," *Sep. Technol.*, **4**, 186 (1994).

Elimelech, M., and C. R. O'Melia, "Effect of Particle Size on Collision Efficiency in the Deposition of Brownian Particles with Electrostatic Energy Barriers," *Langmuir*, **6**, 1153 (1990).

Imdakm, A. O., and M. Sahimi, "Transport of Large Particles in Flow Through Porous Media," *Phys. Rev. A*, **36**, 5304 (1987).

Imdakm, A. O., and M. Sahimi, "Computer Simulation of Particle Transport Processes in Flow Through Porous Media," *Chem. Eng. Sci.*, **46**, 1977 (1991).

Ison, C. R., and K. J. Ives, "Removal Mechanisms in Deep Bed Filtration," *Chem. Eng. Sci.*, **24**, 717 (1969).

Ives, K. J., "Rational Design of Filters," *Proc. Inst. Civil Eng. (London)*, **16**, 189 (1960).

Ives, K. J., "Filtration Using Reduction Algae," *Proc. ASCE, J. Sanitary Eng. Div.*, **87**, No. SA3, 23 (1961).

Johnson, P. R., and M. Elimelech, "Dynamics of Colloid Deposition in Porous Media: Blocking Based on Random Sequential Adsorption," *Langmuir*, **11**, 801 (1995).

Jung, Y., and C. Tien, "Simulation of Aerosol Deposition in Granular Media," *Aerosol Sci. Technol.*, **18**, 418 (1993).

Liu, D., P. R. Johnson, and M. Elimelech, "Colloid Deposition Dynamics in Flow Through Porous Media: Role of Electrolyte Concentration," *Environ. Sci. Technol.*, **29**, 2963 (1995).

Mackie, R. I., R. M. W. Horner, and R. J. Jarvis, "Dynamic Modeling of Deep Bed Filtration," *AIChE J.*, **33**, 1761 (1987).

Maroudas, A., and P. Eisenklam, "Clarification of Suspensions: A Study of Particle Deposition in Granular Media: I. Some Observations on Particle Deposition," *Chem. Eng. Sci.*, **20**, 867 (1965).

McDowell-Boyer, L. M, J. R. Hunt, and N. Sitar, "Particle Transport Through Porous Media," *Water Resour. Res.*, **22**, 1901 (1986).

Michalopoulou, A. C., V. N. Burganos, and A. C. Payatakes, "Creeping Axisymmetric Flow Around a Solid Particle Near a Permeable Obstacle," *AIChE J.*, **38**, 1213 (1992).

Michalopoulou, A. C., V. N. Burganos, and A. C. Payatakes, "Hydrodynamic Interactions of Two Permeable Particles Moving Slowly Along Their Centerline," *Chem. Eng. Sci.*, **48**, 2889 (1993).

Nabzar, L., G. Chauveteau, and C. Roque, "A New Model for Formation Damage by Particle Retention," Int. Symp. on Formation Damage Control, Lafayette, LA (1996).

Paraskeva, C. A., V. N. Burganos, and A. C. Payatakes, "Three-Dimensional Trajectory Analysis of Particle Deposition in Constricted Tubes," *Chem. Eng. Commun.*, **108**, 23 (1991).

Payatakes, A. C., "A New Model for Granular Porous Media. Application to Filtration Through Packed Beds," PhD Diss., Syracuse Univ., Syracuse, NY (1973).

Payatakes, A. C., C. Tien, and R. M Turian, "A New Model for Granular Porous Media— Part I. Model Formulation," *AIChE J.*,, **19**, 58 (1973).

Payatakes, A. C., C. Tien, and R. M Turian, ''Trajectory Calculation of Particle Deposition in Deep Bed Filtration: I. Model Formulation,'' *AIChE J.*, **20**, 889 (1974a).
Payatakes, A. C., R. Rajagopalan, and C. Tien, ''Application of Porous Media Models to the Study of Deep Bed Filtration,'' *Can. J. Chem. Eng.*, **52**, 727 (1974b).
Payatakes, A. C., D. H. Brown, and C. Tien, ''On the Transient Behavior of Deep Bed Filtration,'' AIChE Meeting, Houston, TX (1977).
Payatakes, A. C., H. Y. Park, and J. Petrie, ''A Visual Study of Particle Deposition and Reentrainment During Depth Filtration of Hydrosols with Polyelectrolyte,'' *Chem. Eng. Sci.*, **36**, 1319 (1981).
Pendse, H., C. Tien, and R. M. Turian, ''Dispersion Measurement in Clogged Filter Beds—A Diagnostic Study on Morphology of Particle Deposits,'' *AIChE J.*, **24**, 473 (1978).
Putnam, D. D., and M. A. Burns, ''Predicting the Filtration of Noncoagulating Particles in Depth Filters,'' *Chem. Eng. Sci.*, **52**, 93 (1997).
Rajagopalan, R., and C. Tien, ''Trajectory Analysis of Deep Bed Filtration Using the Sphere-in-Cell Model,'' *AIChE J.*, **22**, 523 (1976).
Rege, S. D., and H. S. Fogler, ''Network Model for Straining Dominated Particle Entrapment in Porous Media,'' *Chem. Eng. Sci.*, **42**, 1553 (1987).
Rege, S. D., and H. S. Fogler, ''A Network Model for Deep Bed Filtration of Solids and Emulsion Drops,'' *AIChE J.*, **34**, 1761 (1988).
Rimer, A. E., ''Filtration Through Trimedia Filter,'' *Proc. ASCE, J. Sanit. Eng. Div.*, **94**, (SA 3), 521 (1968).
Ryan, J. N., and M. Elimelech, ''Colloid Mobilization and Transport in Groundwater,'' *Colloids Surf., A: Physicochem. Eng. Aspects*, **107**, 1 (1996).
Sahimi, M., G. R. Gavalas, and T. T. Tsotsis, ''Statistical and Continuum Models of Fluid-Solid Reactions in Porous Media,'' *Chem. Eng. Sci.*, **45**, 1443 (1990).
Sahimi, M., and A. O. Imdakm, ''Hydrodynamics of Particulate Motion in Porous Media,'' *Phys. Rev. Lett.*, **66**, 1169 (1991).
Sharma, M. M., and Y. C. Yortsos, ''Transport of Particulate Suspension in Porous Media: Model Formulation,'' *AIChE J.*, **33**, 1636 (1987a).
Sharma, M. M., and Y. C. Yortsos, ''A Network Model for Deep Bed Filtration,'' *AIChE J.*, **33**, 1644 (1987b).
Song, L., and M. Elimelech, ''Dynamics of Colloid Deposition in Porous Media: Modeling the Role of Retained Particles,'' *Colloids Surf., A: Physicochem. Eng. Aspects*, **73**, 49 (1993).
Stein, P. C., ''A Study of the Theory of Rapid Filtration of Water Through Sand,'' DSc Diss., Massachusetts Institute of Technology, Cambridge, MA (1940).
Tien C., R. M. Turian, and H. P. Pendse, ''Simulation of the Dynamic Behavior of Deep Bed Filters,'' *AIChE J.*, **25**, 385 (1979).
Tien, C., and A. C. Payatakes, ''Advances in Deep Bed Filtration,'' *AIChE J.*, **25**, 737 (1979).
Tien, C., *Granular Filtration of Aerosols and Hydrosols*, Butterworths, Boston (1989).
Tilton, J. N., and A. C. Payatakes, ''Collocation Solution of Creeping Newtonian Flow Through Sinusoidal Tubes: A Correction,'' *AIChE J.*, **30**, 1016 (1984).
Tsakiroglou, C. D., and A. C. Payatakes, ''A New Simulator of Mercury Porosimetry for the Characterization of Porous Materials,'' *J. Colloid Interf. Sci.*, **137**, 315 (1990).
Tsakiroglou, C. D., and A. C. Payatakes, ''Effect of Pore Size Correlations on Mercury Porosimetry Curves,'' *J. Colloid Interf. Sci.*, **146**, 479 (1991).
Ushiki, K., and C. Tien, ''In-Situ Observation of Aerosol Filtration in a Two-Dimensional Model Filter,'' *Proc. AIChE Annu. Meeting* Symp. Ser., **80**(241), 137 (1984).
Vaidyanathan, R., and C. Tien, ''Hydrosol Deposition in Granular Beds—An Experimental Study,'' *Chem. Eng. Commun.*, **81**, 123 (1989).
Vaidyanathan, R., and C. Tien, ''Hydrosol Deposition in Granular Media Under Unfavorable Surface Conditions,'' *Chem. Eng. Sci.*, **46**, 967 (1991).
Yoshida, H., and C. Tien, ''Dynamic Behavior of Aerosol Filtration in Two-Dimensional Model Filter,'' *Aerosol Sci. Technol.*, **4**, 365 (1985).

Manuscript received May 30, 2000, and revision received Sept. 5, 2000.